



A new insight into the role of rat cytochrome P450 24A1 in metabolism of selective analogs of $1\alpha,25$ -dihydroxyvitamin D_3

Steve Y. Rhieu^{a,b,c}, Andrew J. Annalora^d, Rose M. Gathungu^e, Paul Vouros^e, Milan R. Uskokovic^f, Inge Schuster^g, G. Tayhas R. Palmore^{b,c,h}, G. Satyanarayana Reddy^{a,h,*}

^a Epimer LLC, North Smithfield, RI 02896, USA

^b Division of Biology and Medicine, Brown University, Providence, RI 02912, USA

^c School of Engineering, Brown University, Providence, RI 02912, USA

^d Department of Molecular Biology, The Scripps Research Institute, La Jolla, CA 92037, USA

^e Barnett Institute of Chemical and Biological Analysis and Department of Chemistry and Chemical Biology, Northeastern University, Boston, MA 02115, USA

^f Hoffmann-La Roche Inc., Nutley, NJ 07110, USA

^g Institute of Theoretical Chemistry, University of Vienna, Vienna, Austria

^h Department of Chemistry, Brown University, Providence, RI 02912, USA

ARTICLE INFO

Article history:

Received 13 November 2010
and in revised form 3 February 2011
Available online 19 February 2011

Keywords:

$1\alpha,25$ -Dihydroxyvitamin D_3
 $1\alpha,25$ -Dihydroxy-16-ene-23-yne-vitamin D_3
EB1089
Cytochrome P450 24A1
Molecular docking
Vitamin D metabolism

ABSTRACT

We examined the metabolism of two synthetic analogs of $1\alpha,25$ -dihydroxyvitamin D_3 (**1**), namely $1\alpha,25$ -dihydroxy-16-ene-23-yne-vitamin D_3 (**2**) and $1\alpha,25$ -dihydroxy-16-ene-23-yne-26,27-dimethyl-vitamin D_3 (**4**) using rat cytochrome P450 24A1 (CYP24A1) in a reconstituted system. We noted that **2** is metabolized into a single metabolite identified as C26-hydroxy-**2** while **4** is metabolized into two metabolites, identified as C26-hydroxy-**4** and C26a-hydroxy-**4**. The structural modification of adding methyl groups to the side chain of **1** as in **4** is also featured in another analog, $1\alpha,25$ -dihydroxy-22,24-diene-24,26,27-trihomo-vitamin D_3 (**6**). In a previous study, **6** was shown to be metabolized exactly like **4**, however, the enzyme responsible for its metabolism was found to be not CYP24A1. To gain a better insight into the structural determinants for substrate recognition of different analogs, we performed an *in silico* docking analysis using the crystal structure of rat CYP24A1 that had been solved for the substrate-free open form. Whereas analogs **2** and **4** docked similar to **1**, **6** showed altered interactions for both the A-ring and side chain, despite prototypical recognition of the CD-ring. These findings hint that CYP24A1 metabolizes selectively different analogs of **1**, based on their ability to generate discrete recognition cues required to close the enzyme and trigger the catalytic mechanism.

© 2011 Elsevier Inc. All rights reserved.

Introduction

The active form of vitamin D_3 , $1\alpha,25$ -dihydroxyvitamin D_3 (**1**), is a secosteroid hormone. Aside from its central role in regulating calcium homeostasis, **1** also displays other non-calcemic actions such as antiproliferative and proapoptotic activities against certain types of cancer cells. This finding led to the use of **1** as a possible drug in treatment of renal osteodystrophy, various cancers, and other proliferative disorders such as psoriasis [1–3]. However, the clinical use of **1** is limited mainly because of its side effect of hypercalcemia. To minimize the calcemic effect, numerous vitamin D analogs have been synthesized by adding structural modifications to one or more geographic regions of **1** including the A-ring, seco-B-ring, CD-ring, and/or the side chain as shown in Fig. 1. The

reader is directed to reviews [4–6] for further details on vitamin D analogs.

Some of the structural modifications that are added to **1** are aimed to block metabolic inactivation of **1** so that the therapeutic effects of **1** within target cells can be prolonged. Metabolic inactivation of **1** is catalyzed by mitochondrial cytochrome P450 24A1 (CYP24A1)¹, which is responsible for all the natural metabolites produced through C24, C23, and C26 oxidation pathways [7–10] (Fig. 2).

¹ CYP24A1, cytochrome P450 24A1; IPK, isolated perfused rat kidney; 25(OH) D_3 , 25-hydroxyvitamin D_3 ; $1\alpha,24(R),25(OH)_3D_3$, $1\alpha,24(R),25$ -trihydroxyvitamin D_3 ; $1\alpha,25(OH)_2-24$ -oxo- D_3 , $1\alpha,25$ -dihydroxy-24-oxo-vitamin D_3 ; $1\alpha,23(S),25(OH)_3-24$ -oxo- D_3 , $1\alpha,23(S),25$ -trihydroxy-24-oxo-vitamin D_3 ; $1\alpha,23(OH)_2-24,25,26,27$ -tetranor- D_3 , $1\alpha,23$ -dihydroxy-24,25,26,27-tetranorvitamin D_3 ; $1\alpha,25,26(OH)_3-16$ -ene-23-yne- D_3 , $1\alpha,25,26$ -trihydroxy-16-ene-23-yne-vitamin D_3 ; ADX, adrenodoxin; ADR, adrenodoxin reductase; NADPH, nicotinamide adenine dinucleotide phosphate; HPLC, high-performance liquid chromatography; GC/MS, gas chromatography/mass spectrometry; ESI/MS, electrospray ionization/mass spectrometry; TMS, trimethylsilyl; TMSOH, trimethylsilanol; Chaps, 3-[(3-cholamidopropyl)dimethylammonio]-2-hydroxy-1-propanesulfonate; GA, genetic algorithm.

* Corresponding author. Address: Department of Chemistry, Brown University, Providence, RI 02912, United States. Fax: +1 401 861 9777.

E-mail address: Satya_Reddy@brown.edu (G.S. Reddy).

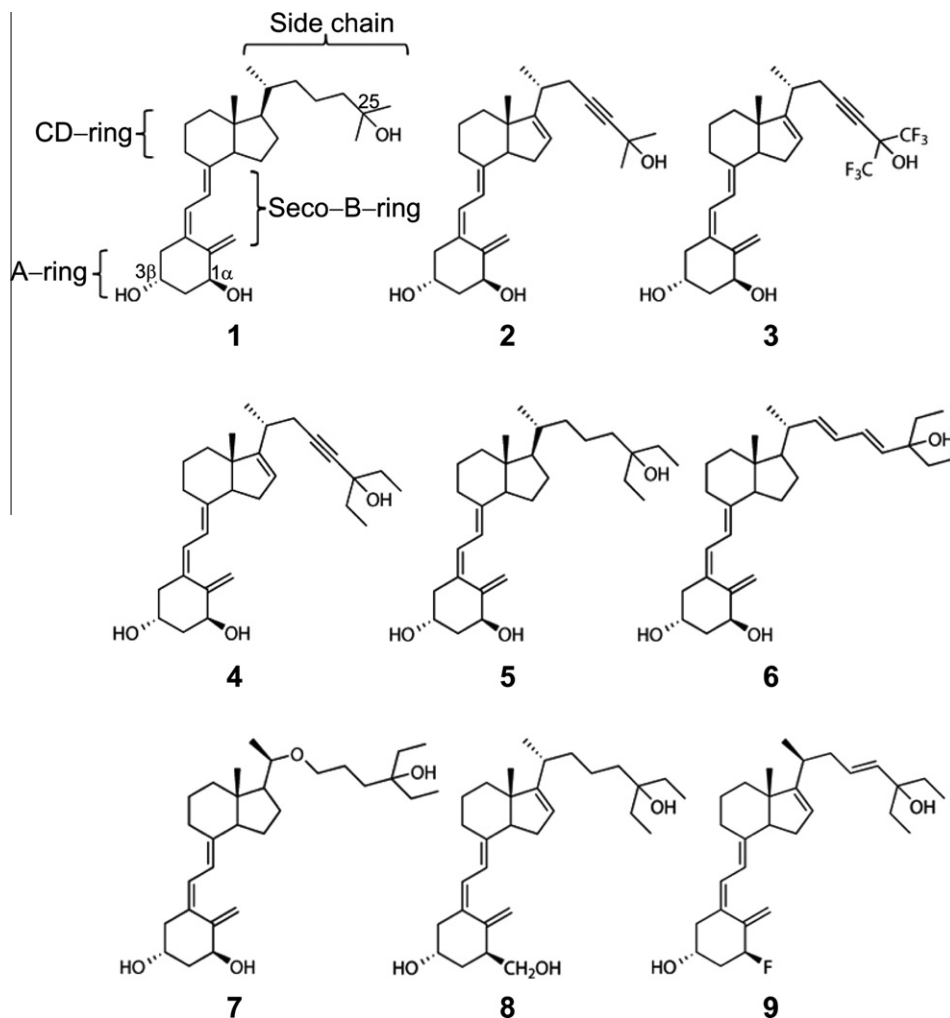


Fig. 1. Chemical structure of $1\alpha,25$ -dihydroxyvitamin D_3 (**1**) and its analogs: $1\alpha,25$ -dihydroxy-16-ene-23-yne-vitamin D_3 (**2**), $1\alpha,25$ -dihydroxy-16-ene-23-yne-hexafluoro-vitamin D_3 (**3**), $1\alpha,25$ -dihydroxy-16-ene-23-yne-26,27-dimethyl-vitamin D_3 (**4**), $1\alpha,25$ -dihydroxy-26,27-dimethyl-vitamin D_3 (**5**), $1\alpha,25$ -dihydroxy-22,24-diene-24,26,27-trihomo-vitamin D_3 or EB1089 (**6**), $1\alpha,25$ -dihydroxy-20-epi-22-oxa-24a-homo-26,27-dimethyl-vitamin D_3 or KH1060 (**7**), 1α -hydroxymethyl- $3\beta,25$ -dihydroxy-16-ene-26,27-bishomo-vitamin D_3 (**8**), and 1α -fluoro-25-hydroxy-16,23E-diene-26,27-bishomo-20-epi-vitamin D_3 (**9**).

Of these metabolic pathways, **1** mainly proceeds through C24 oxidation pathway which is initiated by C24 hydroxylation, followed by a series of side chain oxidations leading to the formation of the final metabolite, calcitric acid [11–13]. The remaining two pathways initiated by C23 and C26 hydroxylations are minor metabolic pathways responsible for conversion of **1** to the final metabolite, calcitriol lactone [14]. For a comprehensive overview on vitamin D metabolism and the enzymes involved, the reader is referred to a recent review [15].

One group of analogs was synthesized with the aim to block metabolic inactivation of **1** through C23 and C24 oxidation pathways by adding 16-ene and 23-yne modifications to **1**. $1\alpha,25$ -dihydroxy-16-ene-23-yne-vitamin D_3 (**2**), the archetype of these analogs, was found to have 4- to 12-fold higher potency than **1** in inducing differentiation and inhibiting proliferation of human myeloid leukemic cells without causing hypercalcemia [16,17]. In a preliminary study, we investigated the metabolism of **2** in an isolated perfused rat kidney (IPK) and noted that **2** is slowly metabolized through only the C26 oxidation pathway resulting in the formation of a minor metabolite which was putatively identified as C26-hydroxy-**2** [18]. We then studied the metabolism of two other 16-ene-23-yne analogs, namely $1\alpha,25$ -dihydroxy-16-ene-23-yne-hexafluoro-vitamin D_3 (**3**) and $1\alpha,25$ -dihydroxy-16-ene-

23-yne-26,27-dimethyl-vitamin D_3 (**4**) in an IPK. Preliminary results indicated that **3** remained unmetabolized [19] while **4** was rapidly metabolized into two polar metabolites (G.S. Reddy, unpublished data). Furthermore, we noted that **2** and **4** were metabolized only in the kidneys isolated from rats that were pretreated with **1**. Since the upregulation of CYP24A1 gene expression and activity by **1** in an IPK is well established [20,21], we speculated that CYP24A1 is the enzyme responsible for the metabolism of **2** and **4**. To prove this hypothesis, we examined the comprehensive metabolism of **2** and **4** using purified rat CYP24A1 in a reconstituted system. We did not include **3** in this study as it remained unmetabolized in an IPK despite highly upregulated CYP24A1. We noted that **2** is metabolized into a single metabolite identified as C26-hydroxy-**2** while **4** is metabolized into two metabolites identified as C26-hydroxy-**4** and C26a-hydroxy-**4**.

The structural modification of extending the distal carbons of the sterol side chain with methyl groups seen in **4** has been incorporated into the synthesis of many other analogs (examples shown in Fig. 1). All these analogs were found to have remarkable biological properties when compared to **1**, for some of them sufficiently promising to enter clinical drug development [22–25]. In particular, analog **6** (EB1089) has been extensively studied including its metabolism [26–30]. It was shown that **6** was metabolized into

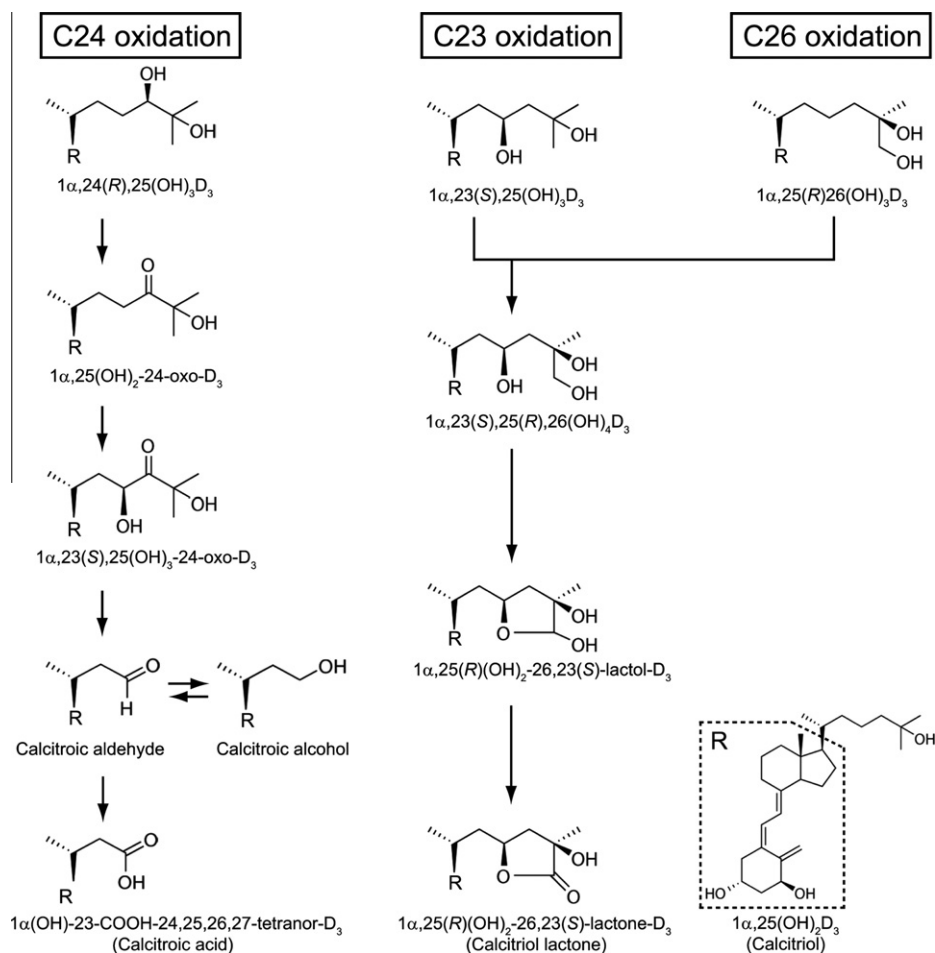


Fig. 2. CYP24A1-mediated metabolism of **1** via C24, C23, or C26 oxidation pathways.

two metabolites identified as C26-hydroxy-**6** and C26a-hydroxy-**6** and the enzyme responsible for its metabolism was not CYP24A1 [27]. To this end, even though the metabolic fate of **4** and **6** are indistinguishable, it is interesting to note that out of the two analogs, only **4** is metabolized by CYP24A1. Recently, the crystal structure of rat CYP24A1 has been published [31]. We took this as an opportunity to gain an insight into the structural determinants of substrate recognition, as a means to understand the metabolic profiles of the analogs **2**, **4**, and **6** by performing a molecular docking analysis.

Materials and methods

Vitamin D compounds and chemicals

Crystalline **1**, **2**, **4**, 25-hydroxyvitamin D₃ (25(OH)D₃), and 1α,25,26-trihydroxy-16-ene-23-yne-vitamin D₃ (1α,25,26(OH)₃-16-ene-23-yne-D₃) were synthesized at Hoffmann-La-Roche (Nutley, NJ). Analog **6** was a generous gift from Dr. J. Welsh (State University of New York at Albany, Rensselaer, NY). All the known natural metabolites of **1** which include 1α,24(R),25-trihydroxyvitamin D₃ (1α,24(R),25(OH)₃D₃), 1α,25-dihydroxy-24-oxo-vitamin D₃ (1α,25(OH)₂-24-oxo-D₃), 1α,23(S),25-trihydroxy-24-oxo-vitamin D₃ (1α,23(S),25(OH)₃-24-oxo-D₃), and 1α,23-dihydroxy-24,25,26,27-tetranorvitamin D₃ (1α,23(OH)₂-24,25,26,27-tetranor-D₃) were biologically synthesized using the IPK as previously described [11]. All other chemicals were purchased from Sigma–Aldrich (St. Louis, MO) and used without further purification.

Preparation of enzymes

Recombinant rat CYP24A1 (WT, Δ2–32) was expressed in *E. coli* (DH5α-FIQ) and purified as described [32]. Purified CYP24A1 samples with A_{417}/A_{280} ratio exceeding 1.0 were considered pure for biochemical assay. Bovine adrenodoxin (ADX) and adrenodoxin reductase (ADR) were expressed and purified as described with minor modifications [32–34]. Spectral purity indexes of ADX (A_{414}/A_{276}) and ADR (A_{452}/A_{278}) used in the present study were 0.9 and 0.1, respectively [32,35]. All enzymes were purified using the AKTA™ FPLC system (GE Healthcare, Chalfont St. Giles, UK) and were stored at –80 °C prior to use.

CYP24A1 reconstitution assay

The CYP24A1 reconstitution assay consisted of a mixture of substrates (5 μM), ADX (0.5 μM), ADR (0.5 μM), and CYP24A1 (0.5 μM) in 1 mL of 50 mM potassium phosphate buffer, pH 7.4. After preincubation at 37 °C for 5 min, the reaction was initiated by adding NADPH at a final concentration of 1 mM. After incubation at 37 °C for 5 min, the reaction was terminated by adding 2 mL of methanol followed by the addition of 1 μg of 25(OH)D₃ as internal standard. The reactants were extracted by adding 4 mL of dichloromethane and subjected to HPLC analysis. A time course study of the metabolism of **2** and **4** was performed in a similar manner as described above except that the buffer contained 0.1 μM ADX, 0.1 μM ADR, and 0.4 μM CYP24A1 over the time period 5–60 min.

Purification of vitamin D metabolites using High-performance liquid chromatography (HPLC)

Lipids were extracted from the enzyme reaction mixture and subjected to HPLC analysis according to a standard procedure [12] using a Waters System Controller (Millennium 3.2). Resolution of vitamin D metabolites was achieved using a Zorbax-SIL column (250 mm × 4.6 mm) (Dupont, Wilmington, DE) eluted with two different solvent mixtures at a flow rate of 2 mL/min: (1) 20% isopropanol in hexane for initial separation (2) 10% isopropanol in hexane for enhanced resolution of the metabolites. A model 996 photodiode array detector (Waters, Milford, MA) was used to monitor lipids with the typical vitamin D chromophore (λ_{\max} at 265 nm and λ_{\min} at 228 nm).

Gas chromatography/Mass spectrometry (GC/MS)

GC/MS analysis was performed using an Agilent GC system 6890 equipped with a mass-selective detector (MSD5973). The metabolites of interest obtained from HPLC were subjected to trimethylsilyl (TMS) derivatization using Power SIL-Prep (Alltech Associates, Deerfield, IL) in anhydrous acetonitrile (50:50, v/v) at 70 °C for 15 min. The derivatized metabolites (final concentration, 10 µg/mL) were subjected to GC/MS analysis using a HP-5MS GC capillary column (30 m × 0.25 mm × 0.25 µm, 5% phenyl siloxane) with helium as a carrier gas at a flow rate of 0.8 mL/min. The oven temperature was set at 150 °C and ramped at a rate of 10 °C/min to reach the final temperature of 300 °C. Full-scan electron impact spectra across the mass range of m/z 50–700 were acquired in each run and the final spectra were obtained after background correction.

Periodate oxidation of vitamin D metabolites

The metabolites of **4** produced by CYP24A1 were purified as described above. Each metabolite (1 µg) in 15 µL of methanol was subjected to treatment with 15 µL of 5% (w/v) sodium periodate at 25 °C for 30 min. The products of the reaction were dried under nitrogen and subjected to HPLC analysis.

Substrate-induced difference spectra

Before proceeding to perform docking analysis, the substrate-induced difference spectra were measured with a Cary Model 500 double-beam spectrophotometer to ensure the ability of **6** to bind to the active site of CYP24A1 along with **1**, **2**, and **4**. After obtaining a baseline with the purified CYP24A1 (0.5 µM) preparation in both reference and sample cuvettes, the vitamin D compounds (1 µM) were added to the sample cuvette while the equal volume of the vehicle solvent (absolute ethanol) was added to the reference cuvette. The final concentration of ethanol was less than 1% (v/v) in all cases.

Ligand docking simulations using AutoDock 4.2

The simulated docking of vitamin D compounds including **1**, **2**, **4**, and **6** into the open conformation of rat CYP24A1 crystal structure (PDB ID: 3K9V, copy A) was performed using AutoDock 4.2 [36,37] with a crystal structure-calibrated docking protocol as described [31]. The topology and parameters for all analogs were generated using the PRODRG server [38] and used as input files for AutoDock 4.2.

Results

Metabolism studies of **1**, **2**, and **4** with an *in vitro* CYP24A1 reconstituted system

In this study, we only investigated the metabolism of **2** and **4** in relation to **1**, but did not include **6** as it was previously shown that **6** was not metabolized by CYP24A1 [27]. The HPLC profiles of lipid soluble metabolites of **1**, **2**, and **4** produced by CYP24A1 are shown in Fig. 3. Within 5 min, extensive metabolism of **1** led to several polar metabolites which were identified as $1\alpha,24(R),25(OH)_3D_3$ (d^*), $1\alpha,25(OH)_2-24-oxo-D_3$ (a^*), $1\alpha,23(S),25(OH)_3-24-oxo-D_3$ (c^*), $1\alpha,23(OH)_2-24,25,26,27-tetranor-D_3$ (b^*), and calcitriol lactone (e^*) based on co-migration with known standards (Fig. 3A). **2** was metabolized into a single metabolite (f^*) while **4** was metabolized into two metabolites (g^* and h^*), all of which were more polar than their respective parent compounds (Fig. 3B and C). The metabolites of **2** and **4** were produced in a quantity sufficient for their structural identification by GC/MS analysis and periodate oxidation. Prior to

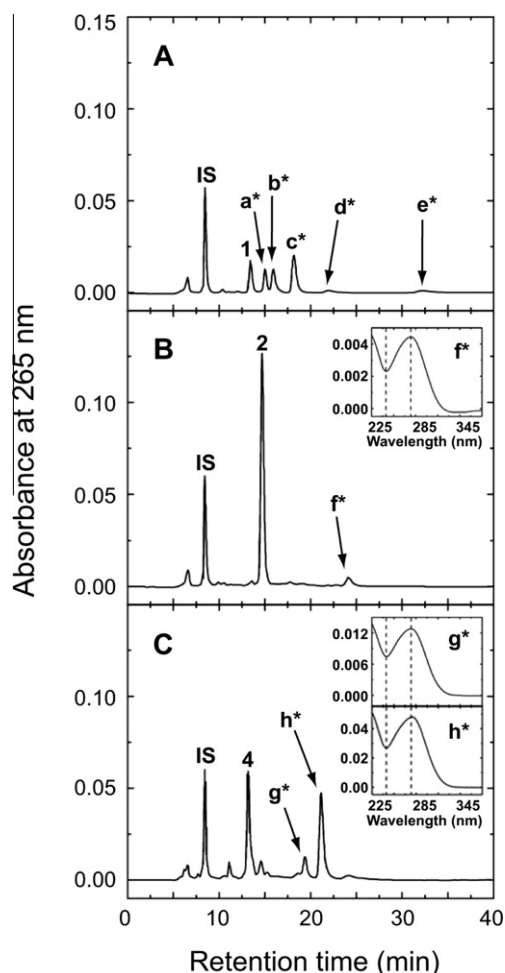


Fig. 3. HPLC profiles of lipid soluble metabolites of **1**, **2**, and **4** produced by CYP24A1. Details of experimental conditions are given in the Methods section. HPLC analysis of lipid extracts of samples was performed using a Zorbax-SIL column (250 mm × 4.6 mm) eluted with 10% isopropanol in hexane at a flow rate of 2 mL/min. 1 µg of $25(OH)D_3$ (IS) was added to each sample before lipid extraction as internal standard to quantify the efficiency of the extraction step. As expected, **1** was metabolized into $1\alpha,24(R),25(OH)_3D_3$ (d^*), $1\alpha,25(OH)_2-24-oxo-D_3$ (a^*), $1\alpha,23(S),25(OH)_3-24-oxo-D_3$ (c^*), $1\alpha,23(OH)_2-24,25,26,27-tetranor-D_3$ (b^*), and calcitriol lactone (e^*) (panel A). **2** was metabolized into a polar metabolite f^* (panel B) while **4** was metabolized into two polar metabolites, g^* and h^* (panel C). All the three polar metabolites possessed the typical vitamin D chromophore showing λ_{\max} at 265 nm and λ_{\min} at 228 nm (inset).

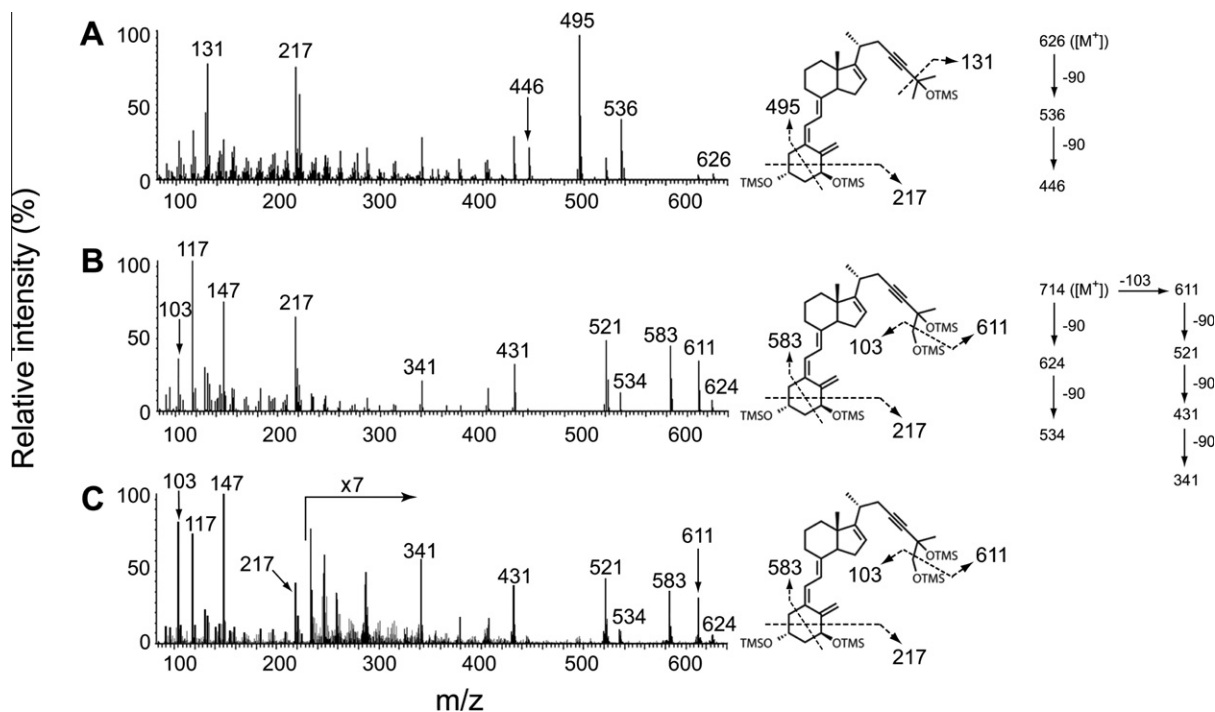


Fig. 4. GC mass spectra of trimethylsilyl derivatives of **2** (A), f^* (B), and synthetic standard of f^* (C). All analyses were performed as described in the Methods section.

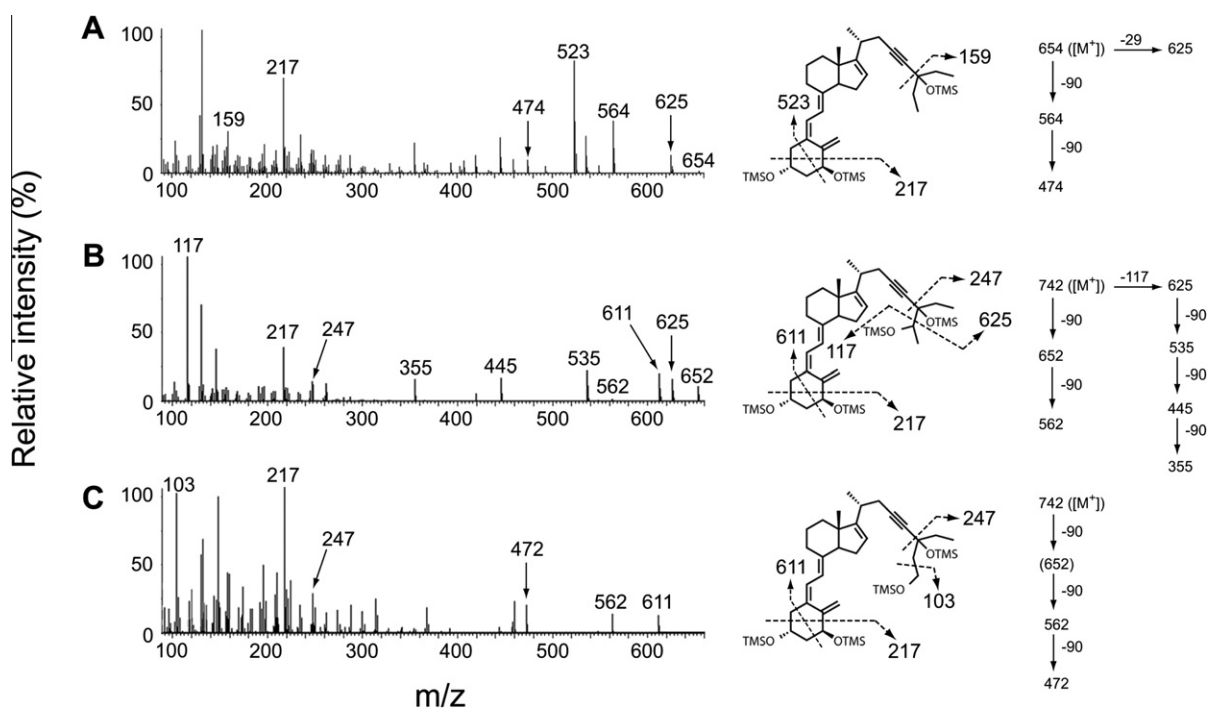


Fig. 5. GC mass spectra of trimethylsilyl derivatives of **4** (A), g^* (B), and h^* (C). Experimental conditions are as described in the Methods section.

GC/MS analysis, the final purity of each compound was tested by its characteristic vitamin D chromophore showing λ_{\max} at 265 nm and λ_{\min} at 228 nm.

Structural identification of metabolite of **2** using GC/MS

The metabolite of **2** was first isolated in our earlier study investigating the metabolism of **2** in an IPK and was identified putatively as C26-hydroxy-**2**. The results of this study were reported only in

an abstract [18]. These preliminary results prompted us to chemically synthesize C26-hydroxy-**2**. Taking advantage of these earlier observations, we proceeded to identify the structure of the metabolite of **2** produced by CYP24A1.

We first obtained the mass spectrum of trimethylsilylated **2** for comparison with that of its metabolite f^* . Its spectrum exhibited the molecular ion ($[M^+]$) at m/z 626 followed by the sequential losses of trimethylsilanol moieties (90 Da) to produce the fragments at m/z 536 and m/z 446. Among other key signature ions

are those involving fragmentations associated with A-ring. Significant are the characteristic fragment ions at m/z 217 (comprised of C1, C2, and C3) and m/z 495 ($[M-131]^+$), involving the loss of C2, C3, and C4, and which serve to establish the integrity of the A-ring (Fig. 4A). Finally, a fragment at m/z 131 is of major structural significance, arising from side chain cleavage across C24–C25 bond. This information provides a template in the interpretation of the spectrum of the metabolite f^* .

The mass spectrum of trimethylsilylated f^* (f^*_{TMS}) exhibited a fragment ion at m/z 624 as its highest detectable mass (Fig. 4B) but did not exhibit the molecular ion peak at m/z 714 since the latter is beyond the mass range of the instrument. However, the molecular mass can be inferred indirectly from consideration of the masses of key fragment ions. Specifically, the presence of a fragment ion at m/z 583 ($[M-131]^+$) can be related to a parent ion of m/z 714. Based on this finding, we concluded that metabolite f^* differed from its parent compound by an additional hydroxyl group. Moreover, fragment ions at m/z 624 ($[M-90]^+$) and m/z 534 ($[M-(90 \times 2)]^+$) reflecting the sequential losses of TMSOH moieties further support the conclusion that they originate from a molecular species of m/z 714. The presence of a fragment ion at m/z 217 was an indication that the integrity of the A-ring is maintained and this ruled out the possibility of A-ring being the site of hydroxylation. The absence of a fragment ion at m/z 131 is indicative of a modification to the end of the side chain. The presence of a fragment ion at m/z 611 ($[M-103]^+$) representing a loss of $[-CH_2OTMS]$ group from the side chain of f^*_{TMS} suggested C26 as the possible site of hydroxylation. A fragment ion at m/z 147 ($[Me_3-Si-O-Si-Me_2]^+$) indicating the presence of two trimethyl-

silyloxy groups in close proximity [39] at C25 and C26, further confirmed C26 as the site of hydroxylation (Fig. 4B). Finally, it should be noted that mass spectral analysis of the trimethylsilylated synthetic standard of $1\alpha,25,26(OH)_3-16-ene-23-yne-D_3$ gave a fragmentation pattern virtually identical to that of f^*_{TMS} (Fig. 4C).

Structural identification of metabolites of **4** using GC/MS

As in the previous case, we first obtained the mass spectrum of trimethylsilylated **4** for comparison with the spectra of its metabolites g^* and h^* . The mass spectrum of trimethylsilylated **4** exhibited a molecular ion ($[M]^+$) at m/z 654, the typical fragments associated with sequential eliminations of TMSOH moieties (m/z 564 and m/z 474), the characteristic fragment ions at m/z 523 ($[M-131]^+$) and m/z 217, arising from A-ring cleavage, and a fragment ion at m/z 159, arising from side chain cleavage across C24–C25 bond (Fig. 5A).

The mass spectra of trimethylsilylated g^* (g^*_{TMS}) and h^* (h^*_{TMS}) exhibited fragment ions at m/z 652 and m/z 611 respectively as their highest detectable masses (Fig. 5B and C) but did not exhibit their molecular ions which are beyond the mass range of the instrument. However, the molecular ion peaks of g^*_{TMS} and h^*_{TMS} at m/z 742 could be inferred indirectly from the presence of the key fragment ion at m/z 611 ($[M-131]^+$) observed in the spectra of both compounds. This conclusion is further corroborated by electrospray ionization/mass spectrum (ESI/MS) results of underivatized **4**, g^* , and h^* which confirm the molecular weight of the metabolites is 16 Da greater than that of the parent compound, **4** (Fig. 6). Based on this finding, we concluded that metabolites g^* and h^* differed from their parent compound by an additional hydroxyl group. The GC/MS spectra of the metabolites exhibited the characteristic fragment ion at m/z 217, which is an indication that the integrity of their A-ring is maintained and thus ruling out the A-ring as the site of hydroxylation. The mass shift of the characteristic fragment ion at m/z 159 in the spectrum of the parent compound to m/z 247 in the spectra of both metabolites suggests that the site of hydroxylation is either C26 or C26a. Fragment ions at m/z 117 and m/z 624 in the spectrum of g^*_{TMS} suggested C26 as the site of hydroxylation (Fig. 5B) while a fragment ion at m/z 103 in the spectrum of h^*_{TMS} suggested C26a as the site of hydroxylation (Fig. 5C). To further confirm the hydroxylation sites in g^*

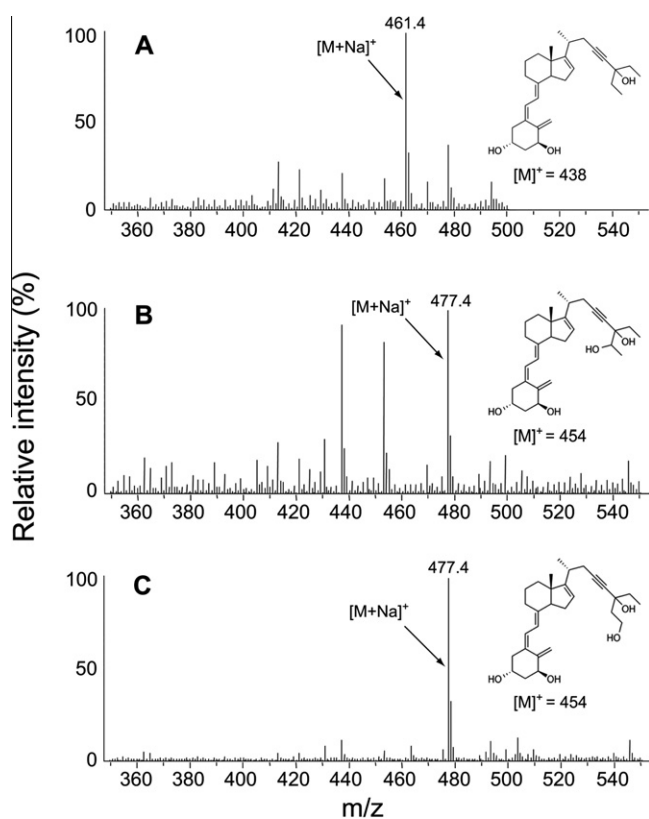


Fig. 6. ESI mass spectra of **4** (A), g^* (B), and h^* (C), whose molecular ion masses ($[M]^+$) are m/z 438, 454, and 454, respectively. Prior to analysis, purified **4**, g^* , and h^* were reconstituted with 0.1% (v/v) formic acid in acetonitrile at final concentrations of 2 $\mu\text{g/mL}$, 1 $\mu\text{g/mL}$, and 2 $\mu\text{g/mL}$, respectively. The sodium adduct ion peak ($[M + Na]^+$) at m/z 477.4 was shown in mass spectra of both g^* and h^* indicating the addition of a hydroxyl group (16 Da) to the parent compound, **4**.

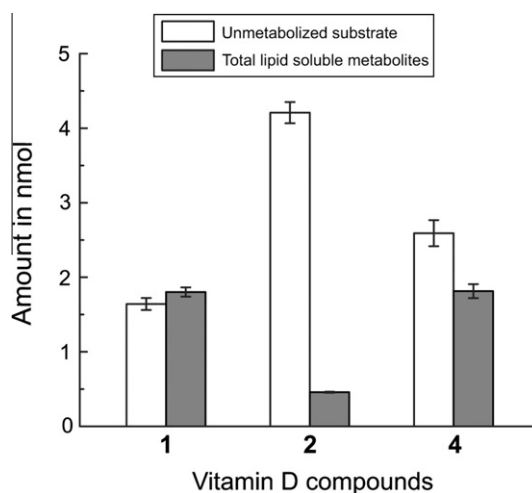


Fig. 7. The relationship between unmetabolized parent compounds **1**, **2**, and **4** and their respective lipid soluble metabolites produced by CYP24A1. Experimental conditions including HPLC analysis are as described in Fig. 3. Metabolites were quantified by integrating the area of the ultraviolet peaks at an absorbance of 265 nm. Error bars represent the mean \pm SD ($n = 4$).

and h^* , both metabolites were subjected to oxidation by sodium periodate. The conversion of g^* into a less polar metabolite suggested that g^* contained a vicinal diol. On the contrary, h^* was found to resist oxidation by sodium periodate (data not shown). Thus, we identified the metabolites of g^* and h^* unequivocally as C26-hydroxy-**4** and C26a-hydroxy-**4**, respectively.

Metabolic stability of **2** over **4**

To examine the metabolic stability of **2** and **4** in relation to **1**, we incubated each compound in 1 mL of CYP24A1 reconstituted system at 5 μ M of concentration. The amounts of the unmetabolized substrate and its metabolites were calculated based on HPLC analysis. The results indicated that 4.2 μ M (84%) of **2** and 2.53 μ M (50.6%) of **4** remained unmetabolized when compared to only 1.64 μ M (32.8%) as in case of **1** (Fig. 7). Thus, both compounds **2** and **4** are more stable when compared to **1**. Following this experiment, we examined the kinetics of disappearance of parent compounds **2** and **4** and generation of their respective metabolites during a period of 60 min. The data indicated a much higher metabolic stability for **2** when compared to **4** (Fig. 8). The higher rate of metabolism of **4** could be attributed to the hydroxylation at C26a generating the metabolite h^* , whereas the hydroxylation at C26 position of both analogs took place practically at identical rates generating the metabolite f^* from **2** and g^* from **4** (Fig. 8B).

Spectral analysis of CYP24A1 induced by substrate binding

As shown in Fig. 9, binding of all tested substrates (**1**, **2**, **4**, and **6**) to CYP24A1 induced a Type I spectral change (peak at \sim 390 nm; trough at \sim 420 nm), indicating the spin state of the heme iron of CYP24A1 is changed from low to high spin. The magnitude of spectral perturbation ($\Delta A_{390-420}$) induced by **1** was larger than that of other substrates. Interestingly, **6**, which is not metabolized by CYP24A1, induced a modest spectral shift similar to **2** and **4**. This finding indicates that **6** can also bind to the active site of CYP24A1 in a configuration that perturbs the heme. However, it has been previously reported that the metabolism of vitamin D substrates by CYP24A1 does not always correlate with the apparent $\Delta A_{390-420}$ [32].

Docking analysis

In comparison to **1**, it was tested whether **2**, **4**, and **6** could achieve substrate-like recognition in the binding pocket of rat CYP24A1, using our recently published computational methods [31]. In Fig. 10A, an idealized model of **1** (shown in yellow) is depicted in the low-energy docking configuration among α -helices

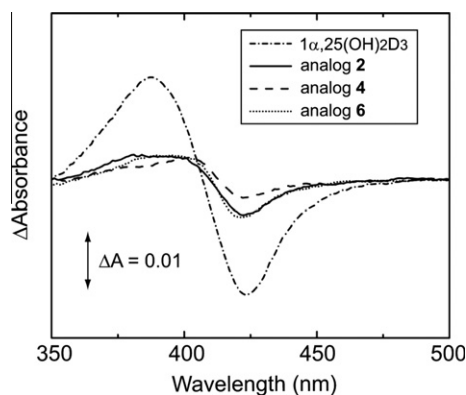


Fig. 9. Substrate-induced difference spectra of rat CYP24A1 with **1**, **2**, **4**, and **6**. The difference spectra of CYP24A1 were measured in 100 mM potassium phosphate buffer (pH 7.4). The concentrations of enzyme and vitamin D compounds used were 0.5 μ M and 1 μ M, respectively.

B', **F**, **G**, **I**, and the β 1–4 sheet. **1** binds to the active site with its side chain positioned over the heme and engages itself in the catalytic center; situated below the structural coordinates of 3-[(3-cholamidopropyl)dimethylammonio]-2-hydroxy-1-propane-sulfonate (Chaps), a zwitterionic detergent used to purify recombinant CYP24A1 that binds tightly to the open form of the enzyme (shown in magenta). In Fig. 10B, the binding site for **1** located below helix F is shown superimposed with the coordinates of Chaps in order to illustrate the proximity of the important substrate-binding residues M246 and F249 [32] to the docking solution of the Chaps binding site. A detailed schematic for the binding configuration of **1**, as seen from below helix F is shown in Fig. 10C.

Complimentary docking studies were performed with **2**, **4**, and **6**. We found that all the analogs were capable of docking the CYP24A1 active site in the same general configuration as **1**. Analog **2** (solution not shown) docked CYP24A1 with six times less computed affinity than **1** (Table 1), and required the CD-ring to rotate between 90° and 180° to accommodate typical hydrogen bonding between the side chain (i.e., 25-OH group) and helix I. However, analog **4** (shown in aqua), which has a bulkier side chain than **2**, docked CYP24A1 normally with only 3-fold lower affinity than **1** (Table 1), and it docked more reproducibly than **2** (Fig. 11A). The docking model for **6** (shown in green), which docked CYP24A1 with more than twice the computed binding affinity of **1** (Table 1), is shown superimposed with the coordinates of **1** in Fig. 11B.

Unlike **6**, analogs **2** and **4** consistently bind the CYP24A1 active site in a configuration similar to **1**, with the side chain positioned over the heme. As depicted in Fig. 11C, the side chain of **4** interacts

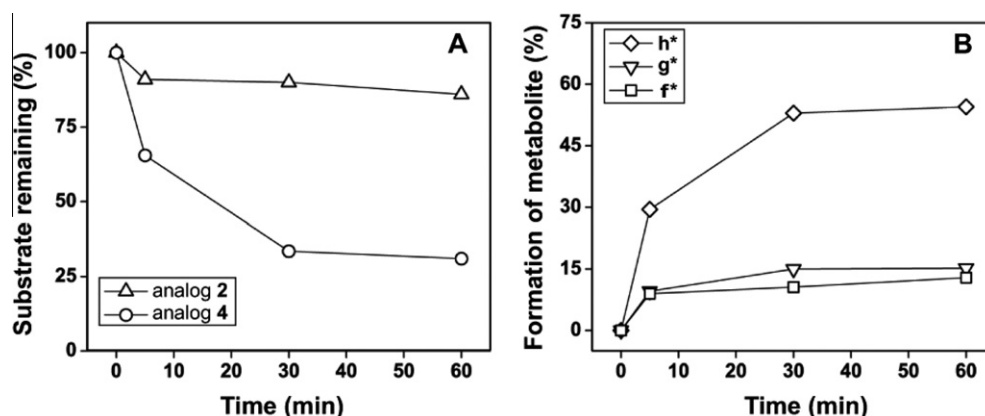


Fig. 8. Time course of the metabolism of **2** and **4** incubated in a CYP24A1 reconstituted system. Experimental conditions are as described in the Methods section.

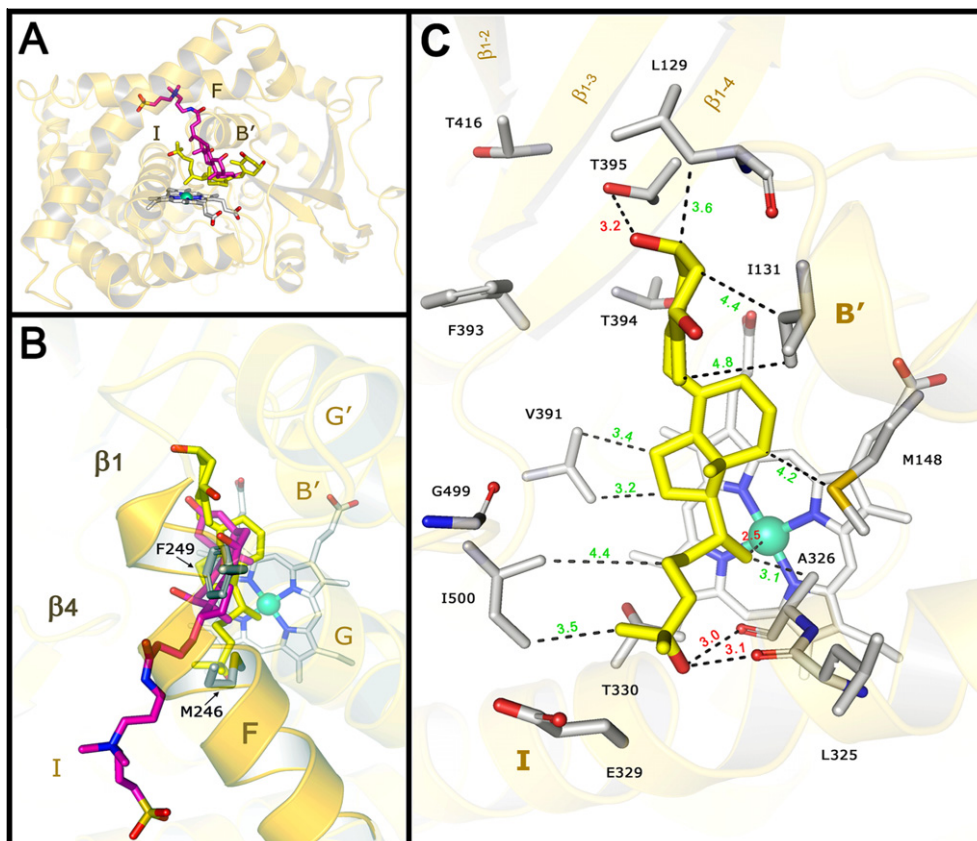


Fig. 10. A computational model of secosteroid recognition in the open structure of CYP24A1. (A) An Autodock 4.2 docking model for the binding of **1** (in yellow) within the heme-centered active site of CYP24A1 is shown (gold ribbon, PDB ID: 3K9V, copy A). **1** reproducibly docked the enzyme's active site formed among helices B', F, G, I, and β 1–4 sheet, in a configuration that positions the 25-hydroxylated side chain over the heme via discrete contacts with the kinked, central helix I. **1** binds deeply in the hydrophobic binding pocket of CYP24A1, below the coordinates of a Chaps detergent molecule (magenta, PDB ID: 3K9V, CPS600) found in the crystal structure. (B) The putative active site of CYP24A1 converges below the hydrophobic pocket formed among helices F, G, and G'. In this conformation, important amino acid residues from helix F (M246 and F249) are well positioned to interact with potential substrates and close the active site cavity. (C) The optimized docking model for **1** is shown interacting with key amino acid residues (shown in gray) from the B-B' loop (L129 and I131), B'-C loop (M148), helix I (L325, A326, E329, and T330), helix K/ β 1–4 loop (V391), β 1–4 sheet (F393, T394, and T395), β 1–3 sheet (T416), and β 4 turn (G499 and I500); notable hydrogen-bond (Å, red) and hydrophobic-bond distances (Å, green) are given with respect to computed atom positions. The docking of **1** is stabilized in the CYP24A1 active site by multiple hydrophobic contacts, and at least 3 hydrogen bonds (i.e., between the 3 β -OH group and β 1–4 sheet, and the 25-OH group and helix I).

with helix I, similar to **1**, within the charged, open cleft that is formed above the heme, among residues L325, A326, A327, V328, E329, and T330. This kinked span of helix I is well hydrated (shown as magenta spheres) in the crystal structure of CYP24A1 [31] and it exposes the main chain atoms of L325 and A326 to solvent at the

Table 1
Flexible ligand docking results for **1**, **2**, **4**, and **6** in the crystal structure of rat CYP24A1.

Ligand ^a	Binding energy ^b [kcal/mol]	Dissociation constant ^c (K_i) [nM]	Occupancy ^d
1	–12.13	1.29	0.16
2	–11.01	8.49	0.12
4	–11.46	3.98	0.20
6	–12.63	0.55	0.18

^a Flexible ligand docking simulations for idealized compounds **1**, **2**, **4**, and **6** were performed using Autodock 4.2. Evaluations were based on experiments consisting of 200 Genetic Algorithm (GA) runs, with long evaluations (25,000,000 evals. per GA run), using a search grid targeting the full distal surface of rat CYP24A1 (PDB ID: 3K9V, copy A).

^b Binding energy is the computed value for the low-energy docking conformation in the high occupancy solution bin (root mean square = 2.0 Å).

^c Dissociation constant or inhibition constant (K_i) is the computed nanomolar affinity for the low-energy, active site binding solution with the highest occupancy.

^d Occupancy refers to the fraction of total docking solutions represented by the low-energy active site docking solution (root mean square = 2.0 Å).

same point where the helix I bends into the heme plane near the catalytic residue T330. Conserved amino acid residues (e.g., Y204, N208, and I215) from helix E engage both sides of the disordered span of helix I, forming the underpinning of an elongated binding pocket that extends the CYP24A1 active site over the heme into a narrowing cavity formed among helices E, F, and I (Fig. 11C). **6** was the only analog tested that could not dock its side chain into the proximal end of CYP24A1's elongated binding pocket.

Discussion

The important role of CYP24A1 in catalyzing the initial hydroxylation at C24 in the metabolism of **1** followed by multiple oxidative reactions leading to the formation of calcitroic acid was established more than two decades ago [11–13,40]. Recent studies [8–10,32,41] have shown that CYP24A1 is responsible for all C24, C23, and C26 oxidation pathways involved in the metabolism of **1** and is responsible for the production of all the metabolites of **1** shown in Fig. 2. Soon after the recognition of CYP24A1 as a multi catalytic enzyme, there have been several studies directed towards understanding the critical role of CYP24A1 in the metabolism of a wide range of synthetic analogs [42–44]. In our present study, we established for the first time the role of CYP24A1 in the metabo-

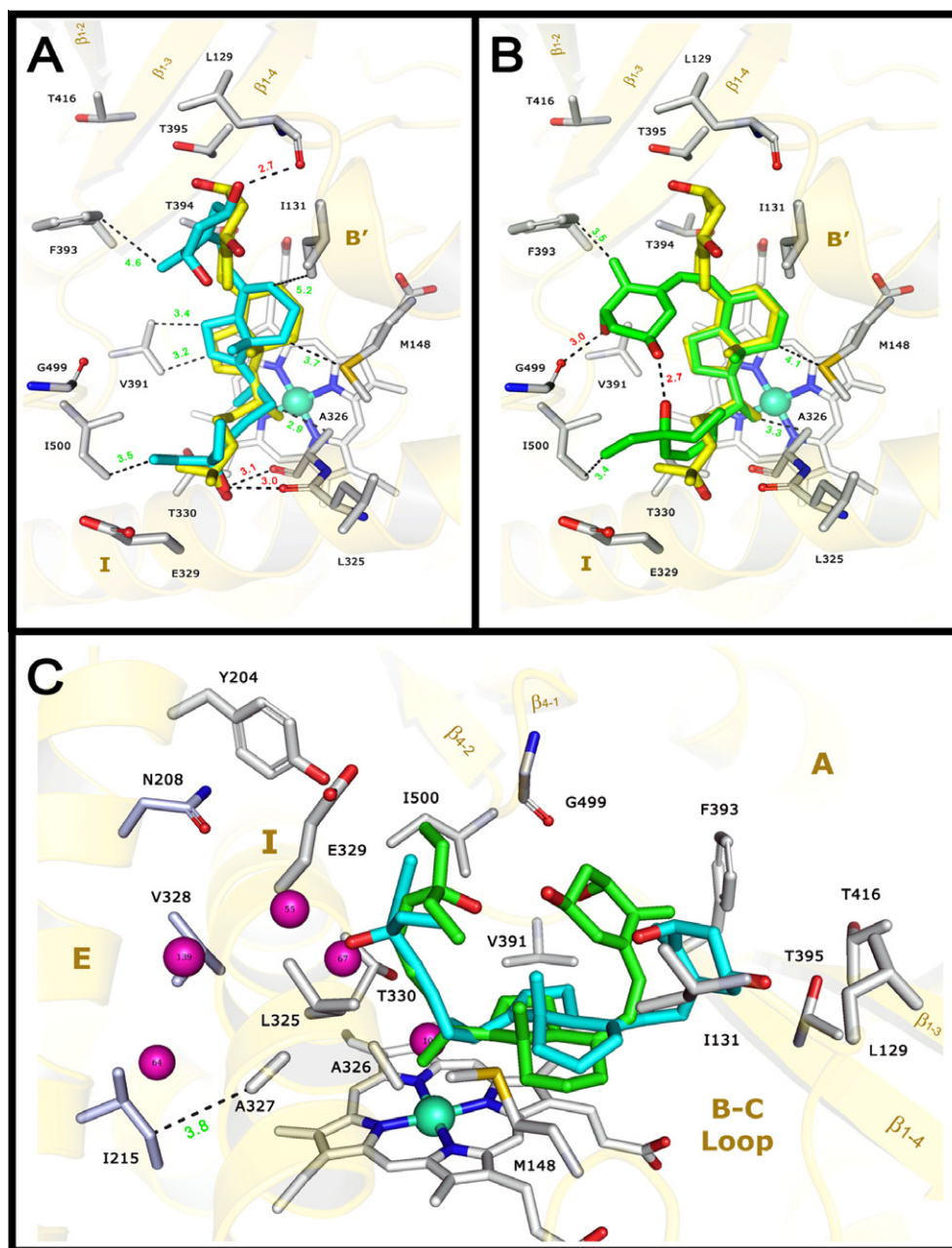


Fig. 11. A comparison of docking results for **1**, **4**, and **6** in the crystal structure of CYP24A1. Low-energy docking solutions for (A) **4** (shown in aqua) and (B) **6** (shown in green) are superimposed with the docking solution for **1** (shown in yellow). Key amino acid residues flanking the substrate-binding pocket are shown and notable hydrogen (A, red) and hydrophobic (A, green) bond distances are given. Analog **6**, which is not metabolized by CYP24A1, docked CYP24A1 with over twice the computed affinity (K_i) of **1**, by forming alternative interactions with the β 1–4 sheet (F393) and the β 4 turn (G499 and I500), which prevent the side chain from forming typical interactions with helix I. In contrast, **4** docked CYP24A1 with seven times less computed affinity than **6**, but appears to be a better mimic of **1**, based on its ability to form alternative contacts with helix I (A326) and the β 4 turn (I500). (C) **4** and **6** are shown superimposed together in the cylindrical active site of CYP24A1, where **4**, but not **6**, can properly dock its bulky side chain over the heme in a putative recognition site centered on an open span of helix I (residues 325–330). This feature may function to recruit the polar functional groups of substrates, as it is stabilized by a string of water molecules in the crystal structure of CYP24A1 (shown as magenta spheres, from 3K9 V, copy A). Multiple conserved residues from helix E (e.g., Y204, N208, and I215) interact with both sides of the kinked span of helix I, as well, helping to form the structural foundation of CYP24A1's extended active site cavity.

lism of two vitamin D analogs **2** and **4** with a common 16-ene-23-yne modification. We showed that **2** is metabolized by CYP24A1 into a single metabolite which is identified as C26-hydroxy-**2**. Thus, it became clear that the presence of a triple bond in the side chain of **2** protects it from undergoing hydroxylations at C23 and C24, but **2** is still subjected to hydroxylation at C26. We noted that **4** is metabolized by CYP24A1 into two metabolites which are unequivocally identified as C26-hydroxy-**4** and C26a-hydroxy-**4**. Out of these two metabolites, C26a-hydroxy-**4** is produced in a

greater quantity (Figs. 3C and 8B), suggesting that the addition of methyl groups to distal carbons of the side chain of **2** renders the analog more susceptible to the action of CYP24A1 (Figs. 7 and 8).

The structural modification of extending the distal carbons of the sterol side chain with methyl groups seen in **4** was introduced for the first time in the synthesis of **5**, which is found to be more potent than **1** in stimulating calcium transport in rachitic rats [45]. This finding of increased biopotency of **5** was assumed to be due to its metabolic stability without direct experimental proof.

Since then, this unique structural modification has been incorporated into the synthesis of several analogs. Some of these analogs shown in Fig. 1, especially **6** gained importance in drug development. Shankar et al. [27] examined the metabolism of **6** in a transformed human keratinocyte cell line (HPK1A-*ras*) and reported that the presence of conjugated double bonds at C22–23 and C24–24a in the side chain of **6** prevents both C23 and C24 hydroxylations, but the distal carbons of the sterol side chain of **6** were subjected to hydroxylations producing metabolites identified as C26-hydroxy-**6** and C26a-hydroxy-**6**. It was also noted that these hydroxylations took place in post-mitochondrial fraction isolated from rat, minipig, and human liver [46]. Furthermore, the incubation of **6** with COS-1 cells transfected with an expression vector containing the cDNA that encodes CYP24A1 produced neither C26 nor C26a hydroxylated metabolites [27]. This implied that CYP24A1 is not responsible for the C26 and C26a hydroxylation of **6**. However, our data from the CYP24A1 reconstitution assay indicated that the enzyme responsible for the C26 and C26a hydroxylations of **4** is CYP24A1. Thus, even though the metabolic fates of **4** and **6** are seemingly identical, it is most interesting to note that the enzymes responsible for their individual metabolism are different. This finding suggested that the structural features utilized by CYP24A1 to hydroxylate **4** but not **6** are probably related to the distance between the ring structure (i.e., CD-ring) and the distal carbons of the side chain as **6** unlike **4** has a longer side chain. However, Dilworth et al. [47] reported that the lengthening of the side chain of **1** has no effect on the activity of CYP24A1 as it is capable of both C23 and C24 hydroxylations of a series of homologated analogs of **1** with their side chains extended up to three additional carbon atoms. Thus, it is interesting to note that the homologation of the side chain as in the case of **6** is not tolerated by CYP24A1 because of the presence of additional modifications in the regions of C23 and C24.

Further understanding of the structural basis by which CYP24A1 discriminates between **1** and analogs **2**, **4**, and **6**, was obtained through our *in silico* docking simulations using the crystal structure of CYP24A1 [31]. We found that all analogs bound to CYP24A1 with the secosteroid nucleus (i.e., CD-ring) in the same general configuration as **1**. But **6** unlike others was the only analog that could not reproducibly dock in a configuration to position its side chain over the heme even though **6** docked with the highest computed affinity (Table 1). Considering the degree of lipophilicity ($\log P$) calculated by ALOGPS 2.1 program [48], such high binding affinity of **6** ($\log P = 6.59$) may be due to having ~10-fold more lipophilicity than **1** ($\log P = 5.51$). Furthermore, we attribute the enhanced binding affinity of **6** to alternative interactions which the A-ring and side chain form with CYP24A1's $\beta 1$ –4 sheet (F393) and $\beta 4$ turn (G499, I500). Out of the analogs **2** and **4** with the common 16-ene-23-yne modification, **4** docked CYP24A1 with ~2-fold higher affinity than **2**, and was a better mimic for **1** with respect to the positioning of the C25 hydroxyl group. It appears that the bulkier side chain of **4** helps to compensate for modifications made to the CD-ring and side chain, by allowing the side chain to form alternative interactions with key binding residues from helix I (A326) and the $\beta 4$ turn (I500). This result helps to explain why CYP24A1 metabolizes **4** more efficiently than **2**, and it also implies that side chain recognition is a key component of CYP24A1's catalytic mechanism. Based on our current understanding of substrate-induced, conformational selection in complex mammalian cytochrome P450s, we speculate that the altered recognition of **6** may impair CYP24A1's ability to acquire a closed form compatible with catalysis [49,50]. This scenario would also apply to analog **2** to a lesser extent, and it provides an alternative explanation for CYP24A1's discrimination between analogs **4** and **6**. New crystal structures of CYP24A1 bound to **1** and its related analogs are needed to clarify the structural basis for this discrete selectivity.

While our docking results do not prove why **6** is not metabolized by CYP24A1, they strongly imply that side chain recognition is a critical component of substrate selectivity in CYP24A1. In this regard, we have identified a putative recognition site for the 25-hydroxylated side chain of known substrates, near the amino acid residues L325 and A326 (helix I) in CYP24A1 (Fig. 10C). This observation is consistent with existing molecular modeling studies of CYP24A1 [51–54], which imply that A326 is a key binding residue that mediates CYP24A1's species-based regioselectivity via interactions with the side chain of **1** [51–53]. In the crystal structure of CYP24A1 [31], a network of water molecules lines the open active site, and they suggest the substrate-binding pocket extends out over the heme center, into an opening formed among helices E, F, and I. The size and positioning of this secondary cavity helps to explain the results of Dilworth et al. [47], who deduced that the CYP24A1 active site must resemble an open cylinder capable of accommodating analogs of **1** with extended side chains, and imply this section of helix I is highly adapted to recruit hydroxylated side chains of increasing length (Fig. 11C). Partial dehydration of this cavity and/or the heme environment may be required to prevent electron uncoupling during catalysis [55,56], and our docking analysis hints that side chain recognition may facilitate this pre-catalytic process. These insights correlate well with previous observations that CYP24A1 requires a hydroxyl group at C25 to introduce the C24 vicinal hydroxyl group, a phenomenon best exemplified by its inability to catalyze the 24(*R*)-hydroxylation of 1α -hydroxyvitamin D₃ [32]. Furthermore, our group previously reported that CYP24A1 can catalyze the C25 hydroxylation of the non-25-hydroxylated synthetic analog, $1\alpha,24$ (*R*)-dihydroxyvitamin D₃ [57]. This work implied that a hydroxyl group at C24 can function as a surrogate for the hydroxyl group at C25. Later, Masuda et al. [58] reported that CYP24A1 can metabolize another non-25-hydroxylated analog, 1α -hydroxyvitamin D₂. Thus the methyl group at C24 in 1α -hydroxyvitamin D₂ can also function as a surrogate for the hydroxyl group at C25. Our analysis hints that CYP24A1 is selective for analogs of **1** that are properly functionalized at either the C24 or C25 position of the side chain.

In summary, we studied the metabolism of two synthetic vitamin D analogs **2** and **4** with a common 16-ene-23-yne modification using rat CYP24A1 in a reconstitution assay. Our finding suggests that the addition of methyl groups at C26/C27 in the side chain of **2** practically made the compound more susceptible to CYP24A1. Similar information with respect to the metabolism of another analog **6** featuring dimethyl groups at its C26/C27 was also provided in a previous study. However, **6** unlike **4** was not metabolized by CYP24A1. These interesting findings provided us an opportunity for the first time to obtain a new insight into the role of CYP24A1 in the metabolism of analogs **4** and **6** by performing an *in silico* docking analysis using the crystal structure of rat CYP24A1. Our results imply that high-affinity binding to CYP24A1 is primarily mediated by hydrophobic contacts with the substrate, but proper recognition, as needed to close the enzyme and initiate the catalytic mechanism, may require discrete interactions between the side chain, properly functionalized either at C24 or C25, and the enzyme's highly evolved helix I.

Acknowledgments

This work was supported by funds from Epimer LLC (G.S.R.) and by a grant (P.V.) from the National Cancer Institute (1R01CA69390). S.Y.R. acknowledges financial support from the NSF GK-12 Teaching Fellowship. A.J.A. thanks Drs. C. David Stout and Eric F. Johnson at the Scripps Research Institute (TSRI) for their support and guidance, and the group at Olson Laboratory and IT services at TSRI for their valuable assistance. This paper is respect-

fully dedicated by Dr. Satya Reddy to Prof. A.W. Norman, who has been his mentor and friend for more than three decades.

References

- [1] E. Abe, C. Miyaura, H. Sakagami, M. Takeda, K. Konno, T. Yamazaki, S. Yoshiki, T. Suda, *Proc. Natl. Acad. Sci. USA* 78 (1981) 4990–4994.
- [2] E.L. Smith, N.C. Walworth, M.F. Holick, *J. Invest. Dermatol.* 86 (1986) 709–714.
- [3] A.S. Dusso, A.J. Brown, E. Slatopolsky, *Am. J. Physiol. Renal Physiol.* 289 (2005) F8–F28.
- [4] R. Bouillon, W.H. Okamura, A.W. Norman, *Endocr. Rev.* 16 (1995) 200–257.
- [5] A.J. Brown, E. Slatopolsky, *Mol. Asp. Med.* 29 (2008) 433–452.
- [6] G. Jones, *Endocrinol. Metab. Clin. North Am.* 39 (2010) 447–472.
- [7] Y. Ohyama, K. Okuda, *J. Biol. Chem.* 266 (1991) 8690–8695.
- [8] M. Akiyoshi-shibata, T. Sakaki, Y. Ohyama, M. Noshiro, K. Okuda, Y. Yabusaki, *Eur. J. Biochem.* 224 (1994) 335–343.
- [9] M.J. Beckman, P. Tadikonda, E. Werner, J. Prah, S. Yamada, H.F. DeLuca, *Biochemistry* 35 (1996) 8465–8472.
- [10] Y. Miyamoto, T. Shinki, K. Yamamoto, Y. Ohyama, H. Iwasaki, R. Hosotani, T. Kasama, H. Takayama, S. Yamada, T. Suda, *J. Biol. Chem.* 272 (1997) 14115–14119.
- [11] R.P. Esvelt, H.K. Schoes, H.F. Deluca, *Biochemistry* 18 (1979) 3977–3983.
- [12] G.S. Reddy, K.Y. Tserng, *Biochemistry* 28 (1989) 1763–1769.
- [13] G. Makin, D. Lohnes, V. Byford, R. Ray, G. Jones, *Biochem. J.* 262 (1989) 173–180.
- [14] J.L. Napoli, R.L. Horst, *Biochem. J.* 206 (1982) 173–176.
- [15] I. Schuster, *Biochim. Biophys. Acta* 1814 (2011) 186–199.
- [16] J.Y. Zhou, A.W. Norman, M. Lubbert, E.D. Collins, M.R. Uskokovic, H.P. Koeffler, *Blood* 74 (1989) 82–93.
- [17] J.Y. Zhou, A.W. Norman, D.L. Chen, G.W. Sun, M.R. Uskokovic, H.P. Koeffler, *Proc. Natl. Acad. Sci. USA* 87 (1990) 3929–3932.
- [18] P.K. Dantuluri, C. Haning, M.R. Uskokovic, K.Y. Tserng, G.S. Reddy, in: A.W. Norman, R. Bouillon, M. Thomasset (Eds.), *Molecular Endocrinology and Clinical Applications*, Walter de Gruyter, Berlin, 1994, p. 32.
- [19] M.R. Uskokovic, A.W. Norman, P.S. Manchand, G.P. Studzinski, M.J. Campbell, H.P. Koeffler, A. Takeuchi, M.L. Siu-Caldera, D.S. Rao, G.S. Reddy, *Steroids* 66 (2001) 463–471.
- [20] G.S. Reddy, G. Jones, S.W. Kooh, D. Fraser, H.F. Deluca, *Am. J. Physiol.* 245 (1983) E359–E364.
- [21] G.S. Reddy, K.Y. Tserng, B.R. Thomas, R. Dayal, A.W. Norman, *Biochemistry* 26 (1987) 324–331.
- [22] K. VanWeelden, L. Flanagan, L. Binderup, M. Tenniswood, J. Welsh, *Endocrinology* 139 (1998) 2102–2110.
- [23] C. Crescioli, P. Ferruzzi, A. Caporali, M. Scaltriti, S. Bettuzzi, R. Mancina, S. Gelmini, M. Serio, D. Villari, G.B. Vannelli, E. Colli, L. Adorini, M. Maggi, *Eur. J. Endocrinol.* 150 (2004) 591–603.
- [24] S. Peleg, F. Khan, N.M. Navone, D.D. Cody, E.A. Johnson, C.S. Van Pelt, G.H. Posner, *J. Steroid, Biochem. Mol. Biol.* 97 (2005) 203–211.
- [25] L. Adorini, G. Penna, S. Amuchastegui, C. Cossetti, F. Aquilano, R. Mariani, B. Fibbi, A. Morelli, M.R. Uskokovic, E. Colli, M. Maggi, *J. Steroid, Biochem. Mol. Biol.* 103 (2007) 689–693.
- [26] K.W. Colston, A.G. Mackay, S.Y. James, L. Binderup, S. Chander, R.C. Coombes, *Biochem. Pharmacol.* 44 (1992) 2273–2280.
- [27] V.N. Shankar, F.J. Dilworth, H.L.J. Makin, N.J. Schroeder, D.J.H. Trafford, A.M. Kissmeyer, M.J. Calverley, E. Binderup, G. Jones, *Biochem. Pharmacol.* 53 (1997) 783–793.
- [28] C.M. Hansen, P.H. Maenpaa, *Biochem. Pharmacol.* 54 (1997) 1173–1179.
- [29] B.L. Lokeshwar, G.G. Schwartz, M.G. Selzer, K.L. Burnstein, S.H. Zhuang, N.L. Block, L. Binderup, *Cancer Epidemiol. Biomarkers Prev.* 8 (1999) 241–248.
- [30] T.R.J. Evans, K.W. Colston, F.J. Lofts, D. Cunningham, D.A. Anthony, H. Gogas, J.S. De Bono, K.J. Hamberg, T. Skov, J.L. Mansi, *Br. J. Cancer* 86 (2002) 680–685.
- [31] A.J. Annalora, D.B. Goodin, W.X. Hong, Q.H. Zhang, E.F. Johnson, C.D. Stout, *J. Mol. Biol.* 396 (2010) 441–451.
- [32] A.J. Annalora, E. Bobrovnikova-Marjon, R. Serda, L. Lansing, M.L. Chiu, A. Pastuszyn, S. Iyer, C.B. Marcus, J.L. Omdahl, *Arch. Biochem. Biophys.* 425 (2004) 133–146.
- [33] Y. Sagara, A. Wada, Y. Takata, M.R. Waterman, K. Sekimizu, T. Horiuchi, *Biol. Pharmacol. Bull.* 16 (1993) 627–630.
- [34] W. Gnanaiah, J.L. Omdahl, *J. Biol. Chem.* 261 (1986) 12649–12654.
- [35] T. Kimura, J.H. Parcells, H.P. Wang, *Methods Enzymol.* 52 (1978) 132–142.
- [36] D.S. Goodsell, A.J. Olson, *Proteins: Struct. Funct. Bioinform.* 8 (1990) 195–202.
- [37] D.S. Goodsell, G.M. Morris, A.J. Olson, *J. Mol. Recognit.* 9 (1996) 1–5.
- [38] A.W. Schuttelkopf, D.M.F. van Aalten, *Acta Crystallogr. Sect. D-Biol. Crystallogr.* 60 (2004) 1355–1363.
- [39] S. Sloan, D.J. Harvey, P. Vouros, *Org. Mass Spectrom.* 5 (1971) 789–799.
- [40] T. Sakaki, N. Sawada, Y. Nonaka, Y. Ohyama, K. Inouye, *Eur. J. Biochem.* 262 (1999) 43–48.
- [41] T. Sakaki, N. Sawada, K. Komai, S. Shiozawa, S. Yamada, K. Yamamoto, Y. Ohyama, K. Inouye, *Eur. J. Biochem.* 267 (2000) 6158–6165.
- [42] T. Kusudo, T. Sakaki, D. Abe, T. Fujishima, A. Kittaka, H. Takayama, M. Ohta, K. Inouye, *Biochem. Biophys. Res. Commun.* 309 (2003) 885–892.
- [43] T. Sakaki, N. Sawada, D. Abe, K. Komai, S. Shiozawa, Y. Nonaka, K. Nakagawa, T. Okano, M. Ohta, K. Inouye, *Biochem. Pharmacol.* 65 (2003) 1957–1965.
- [44] T. Kusudo, T. Sakaki, D. Abe, T. Fujishima, A. Kittaka, H. Takayama, S. Hatakeyama, M. Ohta, K. Inouye, *Biochem. Biophys. Res. Commun.* 321 (2004) 774–782.
- [45] H. Sai, S. Takatsuto, N. Hara, N. Ikekawa, *Chem. Pharm. Bull.* 33 (1985) 878–881.
- [46] A.M. Kissmeyer, E. Binderup, L. Binderup, C.M. Hansen, N.R. Andersen, H.L.J. Makin, N.J. Schroeder, V.N. Shankar, G. Jones, *Biochem. Pharmacol.* 53 (1997) 1087–1097.
- [47] F.J. Dilworth, I. Scott, A. Green, S. Strugnell, Y.D. Guo, E.A. Roberts, R. Kremer, M.J. Calverley, H.L.J. Makin, G. Jones, *J. Biol. Chem.* 270 (1995) 16766–16774.
- [48] I.V. Tetko, V.Y. Tanchuk, *J. Chem. Inf. Comput. Sci.* 42 (2002) 1136–1145.
- [49] N. Mast, M.A. Whitet, I. Bjorkhem, E.F. Johnson, C.D. Stout, I.A. Pikuleva, *Proc. Natl. Acad. Sci. USA* 105 (2008) 9546–9551.
- [50] Y.T. Lee, E.C. Glazer, R.F. Wilson, C.D. Stout, D.B. Goodin, *Biochemistry* 50 (2011) 693–703.
- [51] H. Hamamoto, T. Kusudo, N. Urushino, H. Masuno, K. Yamamoto, S. Yamada, M. Kamakura, M. Ohta, K. Inouye, T. Sakaki, *Mol. Pharmacol.* 70 (2006) 120–128.
- [52] A.J. Annalora, E. Bobrovnikov-Marion, R. Serda, A. Pastuszyn, S.E. Graham, C.B. Marcus, J.L. Omdahl, *Arch. Biochem. Biophys.* 460 (2007) 262–273.
- [53] D.E. Prosser, M. Kaufmann, B. O’Leary, V. Byford, G. Jones, *Proc. Natl. Acad. Sci. USA* 104 (2007) 12673–12678.
- [54] S. Masuda, D.E. Prosser, Y.D. Guo, M. Kaufmann, G. Jones, *Arch. Biochem. Biophys.* 460 (2007) 177–191.
- [55] P.J. Loida, S.G. Sligar, *Biochemistry* 32 (1993) 11530–11538.
- [56] P. Hlavica, *Eur. J. Biochem.* 271 (2004) 4335–4360.
- [57] N. Astecker, E.A. Bobrovnikova, J.L. Omdahl, L. Gennaro, P. Vouros, I. Schuster, M.R. Uskokovic, S. Ishizuka, G. Wang, G.S. Reddy, *Arch. Biochem. Biophys.* 431 (2004) 261–270.
- [58] S. Masuda, S.A. Strugnell, J.C. Knutson, R. St-Arnaud, G. Jones, *Biochim. Biophys. Acta* 1761 (2006) 221–234.